Physiological Tremor Filtering Without Phase Distortion for Robotic Microsurgery

Kabita Adhikari, Sivanagaraja Tatinati, *Member, IEEE*, Kalyana C. Veluvolu, *Senior Member, IEEE*, and Jonathon A. Chambers, *Fellow, IEEE*

***Abstract*— All existing physiological tremor filtering algorithms, developed for robotic microsurgery, use nonlinear phase prefilters to isolate the tremor signal. Such filters cause phase distortion to the filtered tremor signal and limit the filtering accuracy. We revisited this long-standing problem to enable filtering of the physiological tremor without any phase distortion. We developed a combined estimation–prediction paradigm that offers zero-phase type filtering. The estimation is achieved with the mathematically modified recursive singular spectrum analysis algorithm, and the prediction is delivered with the standard extreme learning machine. In addition, to limit the computational cost, we developed two moving window versions of this structure, which are appropriate for real-time implementation. The proposed paradigm preserved the natural phase of the filtered tremor. It achieved the key performance index of error limitation below 10μm, yielding the estimation accuracy larger than 70%, at a time delay of 36 ms only. Both moving window versions of the proposed approach restricted the computational cost considerably while offering the same performance. It is the first time that the effective estimation of the physiological tremor is achieved, without any prefiltering and phase distortion. This proposed method is feasible for real-time implantation. Clinical translation of the proposed paradigm can significantly enhance the outcome in hand-held surgical robotics.**

***Note to Practitioners*—The imprecision caused by physiological hand tremor in microsurgeries has motivated researchers to innovate an efficient tremor compensating technique that can improve surgical performance. Yet, all the existing tremor filtering algorithms, implemented in hand-held surgical instruments, use nonlinear phase prefilters to separate the tremor signal. The inherent phase distortion caused by such prefilters restricts the filtering performance significantly and renders the existing methods inadequate for hand-held robotic surgery. Motivated by this, we proposed a novel estimator-predictor-based framework, by adopting the modified recursive singular spectrum analysis estimator and the extreme learning machine predictor. The proposed framework filters the tremor signal accurately, without distorting it, but at a small fixed lag. In a set of rigorous testing performed by emulating real-time processing, the proposed algorithm showed higher performance compared with the state-of-the-art algorithms. This validates not only its suitability for real-time implantation but also its potential to improve surgical performance, which has been limited by the distorted filtering. Nonetheless, we have presented a proof-of-principle framework for distortion-free filtering, but its full implementation in a real surgical instrument, such as Micron or ITrem, requires a substantial amount of experimental testing and verification. It can be also applicable in a wide range of areas, including healthcare, digital manufacturing, smart automation and control, and various other robotic technologies where efficient filtering of advanced sensor data is highly desirable. In the future, we will develop the multidimensional model of the proposed framework to enable filtering of tremor in the *xyz*-axes simultaneously.**

***Index Terms*— Extreme learning machine (ELM), physiological tremor, recursive singular spectrum analysis (RSSA), robotic microsurgery.**

I. Introduction

PHYSIOLOGICAL tremor is an involuntary and quasi-periodic movement that commonly exists in normal human hand motion [1]. Its frequency spectrum lies in the range of 6–14 Hz [2], [3], and its magnitude can be as high as 100 μm [4]–[7]. This level of oscillation is not so much of a problem for day-to-day tasks but causes detrimental effects in microsurgery that requires precise hand positioning [8], [9]. The undesired vibration of the tip of a surgical tool, caused by natural hand tremor, degrades the efficacy of microsurgical interventions, such as treatment procedures for retinal vascular occlusions or peeling of thin membranes, in which a positioning accuracy of 10 μm, or less, is typically required [10]–[12].

The movement of the tip of a microsurgery tool comprises voluntary motion and involuntary motion that includes the physiological hand tremor, jerk, and low-frequency drift. Among all, the physiological tremor has the most adverse effect on surgical micromanipulation as jerk occurs rarely and drift can be adjusted by visual feedback [13]. To attenuate the physiological hand tremor, there have been remarkable advancements in surgical robotics in last three decades, including telerobotic and robot-assisted systems [14]–[16], steady-hand robotic systems [17], [18], and smart hand-held

Manuscript received April 15, 2020; accepted November 16, 2020. Date of publication December 18, 2020; date of current version January 6, 2022. This article was recommended for publication by Associate Editor K. Suzuki and Editor C. Seatzu upon evaluation of the reviewers' comments. This work was supported in part by Newcastle University, Newcastle, U.K., and in part by the National Research Foundation (NRF) of Korea through the Ministry of Education, Science and Technology under Grant NRF-2018R1A6A1A03025109. *(Corresponding author: Kabita Adhikari.)*

Kabita Adhikari and Jonathon A. Chambers are with the School of Engineering, Newcastle University, Newcastle upon Tyne NE1 7RU, U.K. (e-mail: kabita.adhikari@newcastle.ac.uk).

Sivanagaraja Tatinati is with the School of Electrical and Electronic Engineering, Nanyang Technological University, Singapore 639798.

Kalyana C. Veluvolu is with the School of Electronics Engineering, Kyungpook National University, Daegu 702-701, South Korea.

This article has supplementary material provided by the authors and color versions of one or more figures available at https://doi.org/10.1109/TASE.2020.3041427.

Digital Object Identifier 10.1109/TASE.2020.3041427

surgical devices [2], [3], [19], [20]. Among all, direct-hand surgery still retains its appeal as it provides surgeons' expertise and natural feel and is intuitive due to the fast correspondence between the visual feedback and voluntary hand motion of the surgeon who is directly holding the instrument [2], [6], [16], [21]. Despite these advantages, the high level of hand positioning and dexterity required for microsurgery restricts a number of qualified surgeons due to their natural tremor [19]. Hence, to enhance the dexterity of direct-hand surgery, smart hand-held surgical instruments, such as Micron [2], [19] and ITrem [20], have been developed with the aim to effectively alleviate the physiological tremor from the tip of the instrument.

The voluntary motion of the hand is confined below 4 Hz [22]. Hence, initially, in human–machine interface, linear-phase low- or band-stop filters were applied directly to the whole motion to suppress the tremor [23], [24]. To be effective, these filters require a large filter order that introduces a considerable time delay [25]. Therefore, the use of these filters was discouraged [5], [26]. Riviere *et al.* [2] proposed a smart hand-held device, called Micron, which senses its own motion, isolates the tremor from other components, and then actuates the tip in an equal but opposite direction to cancel the tremor effectively. For the effective performance of Micron, the accurate estimation of the tremor is crucial; otherwise, exact antiphase actuation cannot be accomplished. The amplitude and the spectrum of the tremor are, however, unknown and time-varying. Hence, to track the nonstationary tremor, they utilized an adaptive filtering approach called a weighted Fourier linear combiner (wFLC) [6]. In recent years, wFLC has been extended to autoregressive [27], band-limited [28]–[30], and quaternion [31] versions. To function accurately, all these adaptive techniques required a reference tremor signal, which was generated by prefiltering the whole motion with an infinite impulse response (IIR) filter.

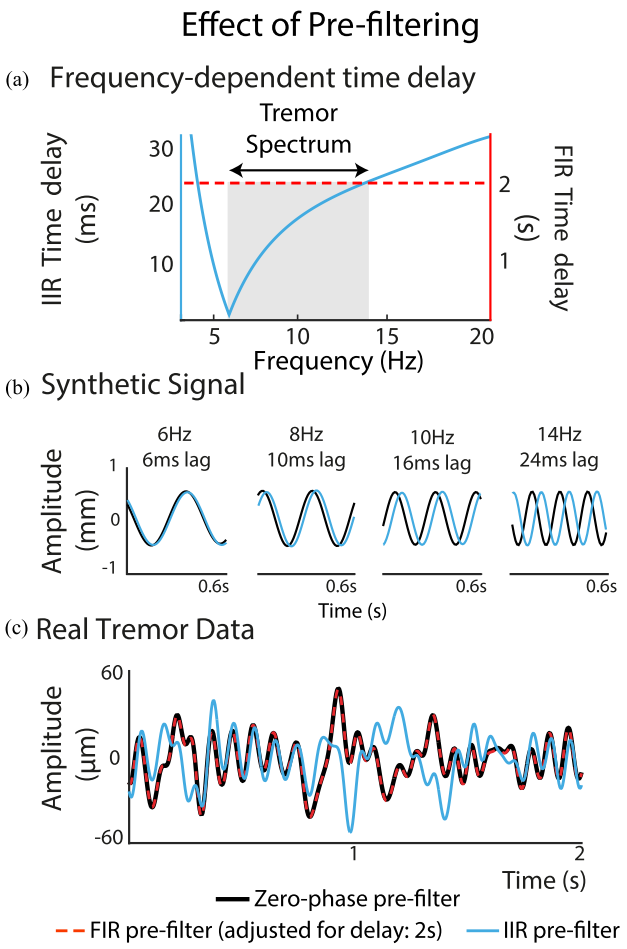

Fig. 1. Effect of prefiltering. (a) Time versus frequency responses of the linear-phase FIR and nonlinear phase IIR prefilters. (b) Frequency-specific phase delay caused by the IIR filter introduced in (a). (c) Reference tremor signal, of a novice surgeon, generated with zero-phase, IIR, and FIR prefilters. Unlike the FIR filter, the IIR prefilter distorts the shape of the tremor signal. The output of the FIR filter is adjusted for the 2-s delay.

A. Detrimental Effect of Prefiltering

The key shortcoming of the wFLC algorithm is caused by the aforementioned prefilter. The time delay introduced by such IIR prefilters is much less compared with the delay introduced by linear phase filters, but they cause frequency-selective delays. Fig. 1(a) shows the time delay versus frequency plot for the fifth-order bandpass Butterworth IIR filter with a passband of 2–20 Hz, which was used in [27], [30], and [32]. In addition, it shows the same for a linear phase Hamming-window-based finite impulse response (FIR) filter with an order of 1000. The IIR filter causes a frequency-specific time delay. However, the FIR filter features a constant time delay of 2 s ($= 1000/2 \times 4$ ms; the sampling time is 4 ms) to all the frequencies in its passband. A time-domain representation of the frequency-specific effect of the above IIR prefilter on four tones in the tremor frequency band is shown in Fig. 1(b).

Fig. 1(c) shows a 2-s plot of a real tremor signal (black) obtained for a novice subject by using a zero-phase prefilter with the same specifications as the IIR prefilters of Fig. 1(a). The IIR prefilter completely distorts the shape of the reference tremor signal. The FIR prefilter accurately approximates the tremor signal; however, the tradeoff is an extremely high delay, which makes it inapplicable for real-time implementation. The resulting frequency-specific distortion of the IIR prefilter limits the efficacy of the wFLC algorithm in real-time implementations. All the off-springs of the wFLC, e.g., [28], [31], and [32], inherit this shortcoming.

To overcome this frequency-specific distortion effect, Veluvolu *et al.* [30] proposed a multistep prediction method with a fixed-horizon. They postulated that, if the exact delay caused by a nonlinear phase filter is preknown, then it can be overcome by using multistep prediction. However, the frequency selective delay experienced by the reference tremor cannot be preknown in real time, as the spectrum of the tremor signal is nonstationary. This was later acknowledged in [32] and [33]. The authors agreed that the limitation of the conventional nonlinear phase filters is their inherent phase distortion. As a solution, they proposed a phase correction technique based on the moving window least-squares support vector machines (MWLSSVMs) and the 1-D online sequential robust extreme learning machine (ELM) (1D-OSRELM) algorithms, which yielded better filtering performance [32],

[33]. These algorithms, however, still relied on IIR prefilters to isolate the tremor signal from the whole motion. As a consequence, the isolated tremor was completely distorted. The distorted tremor signal was then rectified by mapping it with the nondistorted tremor signal obtained from zero-phase filtering. Since the tremor signal is nonstationary, for an accurate rectification, these methods necessitated the tremor signal to be zero-phase filtered continuously to adapt to its changing characteristics. However, the zero-phase filtering is a noncausal system and cannot be performed in real time. This limitation renders the aforementioned methods that are inadequate for real-time implementation. Although frequent off-line mapping can be performed, the filter's transient characteristic restricts the prompt update of the mapping, which degrades the filtering performance significantly.

In this article, we offer a new paradigm to address this problem. Instead of prefiltering the tremor signal, we directly extract the voluntary and the tremor signal from the whole motion by decomposing it. We first extract the voluntary signal and then deduct it from the whole motion to approximate the tremor signal. Our approach comprises two units: 1) an estimator and 2) a predictor. We achieve zero-phase type estimation of voluntary motion by adopting the recursive singular spectrum analysis (RSSA) [34] algorithm. However, this zero-phase estimation comes at the cost of a fixed time delay. To shorten this delay, we append a predictor unit, that is, an ELM [35] to the RSSA estimator. This combined structure is tested with the real physiological tremor data recorded from five novices and four microsurgeons, and the results show that the proposed paradigm: 1) yields zero-phase type filtering of the voluntary and tremor signals without causing any distortion and 2) attenuates the unwanted tremor below 10-μm limit that is desired in microsurgeries. The main contribution of this article is the novel paradigm that can filter the tremor signal as accurately as a high-order linear phase filter, yet within a small processing delay, such as a nonlinear phase filter. Hence, it offers the best of both conventional filters, without the need for any prefiltering or zero-phase filtering. This is the major advantage of the proposed framework compared with the existing state-of-the-art techniques.

This article is organized as follows. Section II provides the theoretical overviews of the SSA and ELM algorithms. In Section III, we present the proposed RSSA-ELM and moving window RSSA-ELM methods. We evaluate the off-line and real-time performance of these algorithms using real tremor data in Section IV. Section V contains a discussion of results. Finally, we conclude this article in Section VI. Preliminary results were reported in [36].

II. Review of Existing Methods

A. Singular Spectrum Analysis

The SSA algorithm decomposes a time series into a number of interpretable components by using singular value decomposition (SVD) of a lag-covariance matrix formed from a time series. The SSA algorithm is computed in two complementary stages: decomposition and reconstruction [34].

1) Decomposition: The decomposition stage comprises two substages, embedding followed by SVD. In the embedding substage, the original 1-D time series $\mathbf{x}_N = [x_1, x_2, \ldots, x_N]$ is reconstructed into a multidimensional series. The multidimensional series is a sequence of L-lagged vectors $\mathbf{x}_i$, which forms the trajectory matrix, $\mathbf{X}_{L\times K} = [\mathbf{x}_1\ \mathbf{x}_2\ \mathbf{x}_3\ \cdots\ \mathbf{x}_K]$, where $\mathbf{x}_1 = [x_1, x_2, \ldots, x_L]^T$, $\mathbf{x}_2 = [x_2, x_3, \ldots, x_{L+1}]^T$, $\mathbf{x}_K = [x_K, x_{K+1}, \ldots, x_N]^T$, and $(.)^T$ denotes the transpose operator. The length of each vector is called the window length, L, which can range between $[2, N-1]$. For a time series of length N, the total number of lagged vectors is $K = N - L + 1$. Following embedding, SVD is performed on the covariance matrix $\mathbf{S} = \mathbf{X}\mathbf{X}^T$. The SVD operation enables the trajectory matrix $\mathbf{X}$ to be represented in terms of its L elementary matrices: $\mathbf{X} = \mathbf{X}_1 + \mathbf{X}_2 + \cdots + \mathbf{X}_L$, where $\mathbf{X_i} = (\lambda_i)^{1/2}\mathbf{u}_i\mathbf{v}_i^T$, λ_i is the ith eigenvalue, and $\mathbf{u}_i$ and $\mathbf{v}_i$ are the ith left and right eigenvectors, respectively.

2) Reconstruction: This step comprises eigentriple grouping and diagonal averaging to reconstruct elementary matrices $\mathbf{X}_i$. First, the trajectory matrix for the desired signal is constructed from one or more elementary matrices. The SVD splits the time series into several groups $I = (i_1, i_2, \ldots, i_g)$ with g being the number of eigenvalues. The resultant trajectory matrix of the desired signal is

$$\hat{\mathbf{X}}_I = \sum_{j=i_1}^{i_g} \mathbf{X}_j = \begin{bmatrix} \hat{x}_{11} & \hat{x}_{12} & \hat{x}_{13} & \cdots & \hat{x}_{1K} \\ \hat{x}_{21} & \hat{x}_{22} & \hat{x}_{23} & \cdots & \hat{x}_{2K} \\ \hat{x}_{31} & \hat{x}_{32} & \hat{x}_{33} & \cdots & \hat{x}_{3K} \\ \vdots & \vdots & \vdots & \vdots & \vdots \\ \hat{x}_{(L-1)1} & \hat{x}_{(L-1)2} & \hat{x}_{(L-1)3} & \cdots & \hat{x}_{(L-1)K} \\ \hat{x}_{L1} & \hat{x}_{L2} & \hat{x}_{L3} & \cdots & \hat{x}_{LK} \end{bmatrix}_{L\times K}.$$

The second step is diagonal averaging. Unlike $\mathbf{X}$, the matrix $\hat{\mathbf{X}}_I$ is not a Hankel matrix. Hence, the antidiagonal elements of $\hat{\mathbf{X}}_I$ are averaged to obtain an accurate estimation of each sample. The reconstructed desired series is expressed as $\hat{\mathbf{x}}_N = [\hat{x}_1, \hat{x}_2, \hat{x}_3, \ldots, \hat{x}_N]$, where

$$\begin{cases} \hat{x}_1 = \hat{x}_{11} \\ \hat{x}_2 = (\hat{x}_{12} + \hat{x}_{21})/2 \\ \vdots \\ \hat{x}_{L-1} = (\hat{x}_{(L-1)1} + \hat{x}_{(L-2)2} + \cdots + \hat{x}_{1(L-1)})/(L-1) \\ \hat{x}_L = (\hat{x}_{L1} + \hat{x}_{(L-1)2} + \cdots + \hat{x}_{1L})/L \\ \vdots \\ \hat{x}_K = (\hat{x}_{L(N-2L+2)} + \hat{x}_{(L-1)(N-2L+3)} + \cdots + \hat{x}_{1K})/L \\ \hat{x}_{K+1} = (\hat{x}_{L(N-2L+3)} + \hat{x}_{(L-1)(N-2L+4)} + \cdots + \hat{x}_{2K})/(L-1) \\ \vdots \\ \hat{x}_{N-1} = (\hat{x}_{L(K-1)} + \hat{x}_{(L-1)K})/2 \\ \hat{x}_N = \hat{x}_{LK}. \end{cases}$$

Any sample can be estimated accurately only when an L number of antidiagonal elements are averaged. For example, $\hat{x}_{L-1}$ and $\hat{x}_{K+1}$ are calculated by averaging $L-1$ elements

and are less accurate compared with their adjacent samples $\hat{x}_L$ and $\hat{x}_K$, respectively. The accuracy reduces as the number of antidiagonal elements, representing that the same instant decreases; hence, $\hat{x}_1$ and $\hat{x}_N$ are the most erroneous samples. These $L-1$ samples at the two ends form the transition phase of SSA and are discarded in batch filtering. The rest of the $N-2L-2$ samples are accurate and possess zero-phase characteristics.

B. Extreme Learning Machine

For the prediction of voluntary motion, we adopted the ELM algorithm as it can learn the underlying relationship between an input and an output vector in a random feature space efficiently. The learning of the ELM algorithm is 1000 times faster than the state-of-the-art algorithms, such as support vector machines, with comparable or even better generalization performance [35], [37]. Hence, it has been frequently employed in a wide range of industrial applications [38]–[41]. Briefly, if a training set includes N distinct input, $\mathbf{x}_i \mid \in \mathbb{R}^m$, and target, $\mathbf{t}_i \mid \in \mathbb{R}^n$, vectors, the ELM algorithm performs a nonlinear mapping as

$$f_{\tilde{N}}(\mathbf{x}_j) = \sum_{i=1}^{\tilde{N}} \beta_i g_i(\mathbf{w}_i \cdot \mathbf{x}_j + b_i) = \hat{\mathbf{t}}_j, \text{ for } j = 1, \ldots, N \tag{1}$$

where $\tilde{N}$ is the number of hidden neurons, $\hat{\mathbf{t}}_j$ is the predicted target signal, $g_i(.)$ is the activation function, and $\mathbf{w}_i = [w_{i1}, w_{i2}, \ldots, w_{im}]^T$ is the output weight vector that links the ith hidden neuron to input vector $\mathbf{x}$. Furthermore, $\boldsymbol{\beta}_i = [\beta_{i1}, \beta_{i2}, \ldots, \beta_{in}]^T$ represents the output weight vector that links the ith hidden neuron to output vector $\mathbf{t}_i$, and b_i is the ith hidden layer bias. The N equations of (1) can be written as $\mathbf{H}\boldsymbol{\beta} = \mathbf{T}$, where $\mathbf{H}$ is a hidden layer output matrix, $\boldsymbol{\beta}$ is the output weight matrix, and $\mathbf{T}$ is the target matrix.

III. Proposed Methods

A. RSSA: Zero-Phase Estimator

In batch processing, the covariance matrix formed by N number of samples is decomposed to extract the desired voluntary and tremor signal from the whole motion. To use the SSA algorithm in real time, when the $(N+1)$th sample arrives, the covariance matrix is amended to form the weighted covariance matrix, $\mathbf{S}_{\mathbf{w}}(N')$, which corresponds to the inclusion of an additional column, namely the $(K+1)$th lagged vector [42]. Therefore, when the $(N+i)$th sample arrives, $\mathbf{S}_{\mathbf{w}}(N')$ is updated as follows [42]:

$$\mathbf{S}_{\mathbf{w}}(N') = (1-\gamma)\mathbf{S}_{\mathbf{w}}(N'-1) + \gamma\, \mathbf{x}_{K'}\mathbf{x}_{K'}^T \tag{2}$$

where $N' = N+i$, $K' = K+i$, $\gamma = 1/N'$ is a forgetting factor, and $\mathbf{x}_{K'}$ is the last column of the trajectory matrix $\mathbf{X}$. After eigentriple grouping, the reconstructed matrix will be

$$\hat{\mathbf{X}}_I = \begin{bmatrix} \hat{x}_{11} & \hat{x}_{12} & \hat{x}_{13} & \ldots & \hat{x}_{1K'} \\ \hat{x}_{21} & \hat{x}_{22} & \hat{x}_{23} & \ldots & \hat{x}_{2K'} \\ \hat{x}_{31} & \hat{x}_{32} & \hat{x}_{33} & \ldots & \hat{x}_{3K'} \\ \vdots & \vdots & \vdots & \vdots & \vdots \\ \hat{x}_{(L-1)1} & \hat{x}_{(L-1)2} & \hat{x}_{(L-1)3} & \ldots & \hat{x}_{(L-1)K'} \\ \hat{x}_{L1} & \hat{x}_{L2} & \hat{x}_{L3} & \ldots & \hat{x}_{LK'} \end{bmatrix}_{L\times K'}. \tag{3}$$

At this instance, addition of the $K^{'}$th column in the reconstructed matrix $\hat{\mathbf{X}}_I$ only contributes to the accuracy of the last L samples from $\hat{x}_{K'}$ to $\hat{x}_{N'}$. However, the last $L-1$ samples from $\hat{x}_{K'+1}$ to $\hat{x}_{N'}$ are in a transition phase; the latest sample, which can be estimated accurately with diagonal averaging at this instance, is the $K^{'}$th sample, $\hat{x}_{K'}$. Hence, to obtain zero-phase filtered characteristics, we apply the RSSA algorithm with an $L-1$ sample lag and estimate the $K^{'}$th sample at each iteration.

B. RSSA-ELM

The RSSA algorithm decomposes the whole hand motion into dominant voluntary and several oscillatory tremor components. The power of the voluntary motion in the 0–4-Hz range is significantly larger than that of the tremor components. Initially, we perform an off-line SSA on the first N samples to decompose the whole motion. Then, we apply the fast Fourier transform (FFT) on the first few reconstructed components with dominant power to automatically group all voluntary components below 4 Hz with the dominant power. The use of FFT for automatic grouping of SSA decomposed electroencephalogram signal has been also discussed in [43]. When the $(N+1)$th sample arrives, the RSSA algorithm activates to estimate $N+1$ data samples, out of which the last $L-1$ transient samples are corrupted. This way, the RSSA algorithm provides suitable zero-phase type estimation but suffers from $L-1$ sample delay. To minimize this delay, we cascade an ELM predictor with RSSA, as shown in Fig. 2. For prediction, the last $L-1$ corrupted samples are segregated for testing, and the rest of the initial uncorrupted samples are used for training. While reconstructing the samples at each RSSA iteration, only the last L samples are estimated by averaging. The accuracy of the rest of the initial samples cannot be any further improved by averaging, as we do not get any additional elements representing those initial samples with the addition of a new column, as shown in (3). Hence, except for the last L samples, all samples are copied from the previous iteration.

The ELM provides the mapping between input feature space and target space such that each element in target space is q samples ahead of the corresponding input feature space element, that is, $\tilde{\mathbf{t}}_t = \tilde{\mathbf{x}}_{t-q}$. The input feature space matrix and target space vector are formulated for both training and testing data. The input feature space matrix is formed by a sequence of delayed target vectors such that $\tilde{\mathbf{X}}_t = [\tilde{\mathbf{x}}_t, \tilde{\mathbf{x}}_{t-1}, \ldots, \tilde{\mathbf{x}}_{t-p}]$, where $\tilde{\mathbf{x}}_t$ is the vector that is a q sample delayed version of the target space vector $\tilde{\mathbf{t}}_t$ and p is the size of the feature space. The output weight matrix obtained by the nonlinear mapping implemented in the training phase is used for the q sample

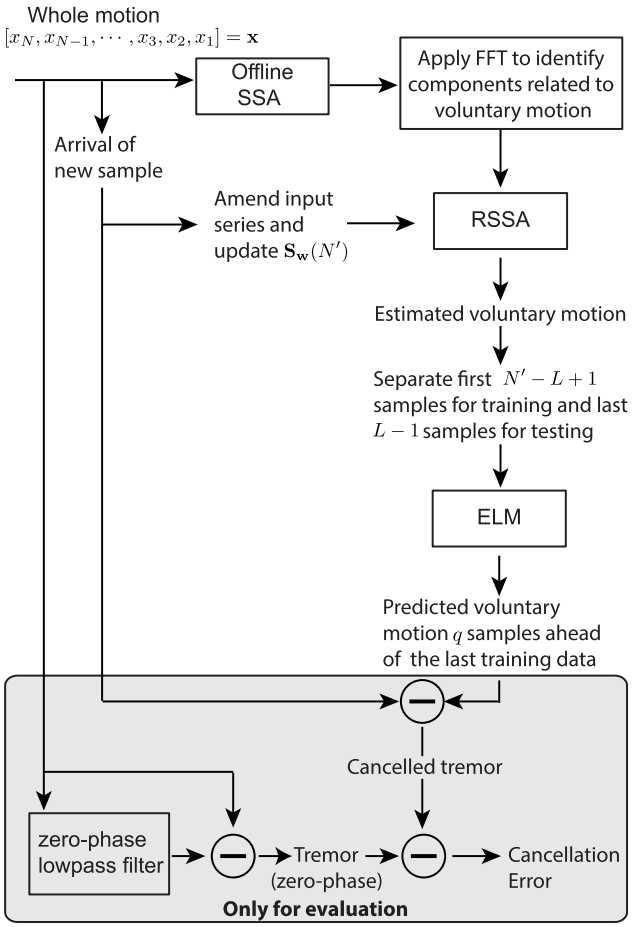

Fig. 2. Functional block diagram of the proposed RSSA-ELM algorithm. RSSA estimates N' samples of the voluntary motion, of which the first $N'-L+1$ are accurate and the last $L-1$ are in the transient phase. The ELM algorithm predicts q samples ahead to shorten the transient phase. The approximated voluntary motion is deducted from the whole motion to obtain the tremor.

ahead prediction of the data samples in the testing phase. The steps for the proposed method are described in Algorithm 1.

C. Two Moving Window RSSA-ELM Variants

To restrict the computational time for each iteration, we propose a method that is a moving window RSSA-ELM, denoted with MW RSSA-ELM. In the MW RSSA-ELM setting, when the $(N+1)$th sample arrives, the first sample is discarded, and then, the $(N+1)$th sample is appended to the data series. Similarly, when the N'th sample arrives such that $N' = N+i$, the time series is updated as $\mathbf{x} = [x_{i+1}, x_{i+2}, \ldots, x_{N'}]^T$. Hence, the size of $\mathbf{X}$ remains fixed, that is, $(L \times K)$. After application of the SVD and grouping, the resultant trajectory matrix is

$$\hat{\mathbf{X}}_I = \begin{bmatrix} \hat{x}_{(i+1)1} & \hat{x}_{(i+1)2} & \hat{x}_{(i+1)3} & \cdots & \hat{x}_{(i+1)K} \\ \hat{x}_{(i+2)1} & \hat{x}_{(i+2)2} & \hat{x}_{(i+2)3} & \cdots & \hat{x}_{(i+2)K} \\ \hat{x}_{(i+3)1} & \hat{x}_{(i+3)2} & \hat{x}_{(i+3)3} & \cdots & \hat{x}_{(i+3)K} \\ \vdots & \vdots & \vdots & \vdots & \vdots \\ \hat{x}_{(i+L-1)1} & \hat{x}_{(i+L-1)2} & \hat{x}_{(i+L-1)3} & \cdots & \hat{x}_{(i+L-1)K} \\ \hat{x}_{(i+L)1} & \hat{x}_{(i+L)2} & \hat{x}_{(i+L)3} & \cdots & \hat{x}_{(i+L)K} \end{bmatrix}_{L \times K}. \quad (4)$$

Algorithm 1 Proposed RSSA-ELM Algorithm

1: Perform batch SSA of a time series with the first N samples - here 8 s.
2: Perform FFT to identify components related to voluntary motion for automatic grouping.
3: When a new sample arrives, append it to the existing time series and activate RSSA.
4: Estimate only the last L samples of the voluntary motion by averaging and copy the first $N'-L$ estimated samples from the previous operation. *Note N' is the dynamic length of the time series and $N' = N+1$ for the 1^{st} RSSA iteration.*
5: Separate the initial $N'-L+1$ samples as training data and the last $L-1$ samples as testing data.
6: Formulate feature space matrices $\tilde{\mathbf{X}}_{t_{train}}$ and $\tilde{\mathbf{X}}_{t_{test}}$ and target space vectors $\tilde{\mathbf{t}}_{t_{train}}$ and $\tilde{\mathbf{t}}_{t_{test}}$ for both training and testing data.
7: Randomly generate the input weight vector $\mathbf{w}$ and hidden layer input biases b.
8: Calculate the hidden layer output matrix, $\mathbf{H}_{train}$ for training data, output weight matrix $\boldsymbol{\beta}$, and hidden layer output matrix, $\mathbf{H}_{test}$ for testing data.
9: Predict q sample ahead target $\hat{\mathbf{t}}_t$ using $\mathbf{H}_{test}$ and $\boldsymbol{\beta}$ with $\mathbf{H}_{test}\boldsymbol{\beta} = \mathbf{T}$ and deduct $\hat{\mathbf{t}}_t$ from the whole motion to obtain the tremor signal.
10: When a new sample arrives repeat from step 3.

In the MW RSSA-ELM method, every time RSSA is performed, all the N samples are estimated by diagonal averaging as in the conventional RSSA [42]. Moreover, we developed the second version of the MW RSSA-ELM and called it Enhanced MW RSSA-ELM. In this method, the initial $N-L$ samples, $\hat{x}_{i+1}$ to $\hat{x}_{i+K-1}$, are copied from the previous iteration, and only the last L samples, $\hat{x}_{i+K}$ to $\hat{x}_{N'}$, are estimated by averaging. By doing so, the first $L-1$ samples are averaged with L antidiagonal elements when the RSSA window is shifted $L-1$ times. Hence, these samples are accurately estimated and are no longer in the transition phase. This approach not only saves significant computational time but also improves the accuracy of the first $L-1$ samples at each iteration simultaneously.

D. Performance Indices

The efficacy of the proposed algorithms was evaluated with the root mean square error (RMSE) that quantifies the remaining uncompensated residual tremor after the estimation. For N data samples, assuming that x_k is the kth sample of the original data, $\hat{x}_k$ is the kth predicted sample, and then, the RMSE is defined as

$$\text{RMSE} = \sqrt{\sum_{k=1}^{N}(x_k - \hat{x}_k)^2/N}.$$

In microsurgeries, it is crucial to suppress the undesired tremulous vibration below 10 μm; hence, RMSE of 10 μm is set as the required threshold for performance evaluation.

RMSE above this level implies failure to achieve the required compensation.

In addition, we calculated Accuracy (%) that quantifies the percentage match between the actual and estimated tremor signals and is defined as

$$\text{Accuracy (\%)} = \frac{\text{rms}(X) - \text{RMSE}}{\text{rms}(x_k)} \times 100$$

where $\text{rms}(X)$ is the root mean square of the original data series X and is defined as $\text{rms}(X) = (\sum_{k=1}^{N} x_k^2/N)^{1/2}$.

Given the RMSE limit of 10 μm, for this data set, the required threshold of Accuracy (%) is 70%, as previously validated in [32] and [33]. Accuracy (%) obtained below this level signifies a failure to achieve the required estimation. Throughout this article, all reported performance measures are averaged across the x-, y-, and z-axes.

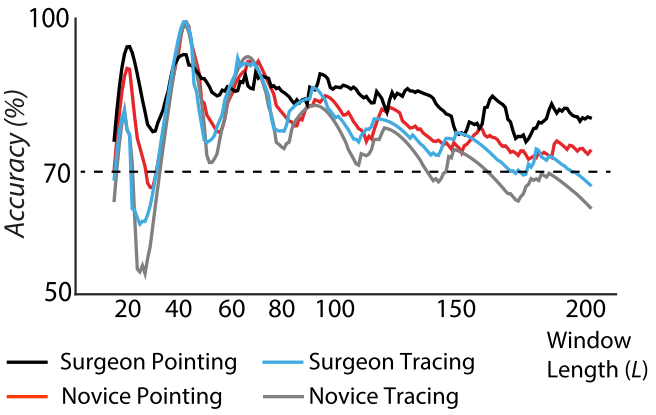

Fig. 3. Accuracy (%), averaged across all subjects versus L. The dashed line shows the minimum acceptable accuracy of 70%.

IV. Results

A. Recording of Physiological Tremor Data

1) Participants: Five medical students with basic surgical skills (novice subjects) and four experienced surgeons (surgeon subjects) were recruited. All the subjects provided informed written consent prior to their participation. The study was approved by the local ethics committee at Nanyang Technological University (NTU) [44].

2) Measurement: With the aim to develop an intelligent hand-held instrument capable of canceling the physiological hand tremor during microsurgery, the researchers from the Biorobotics Lab, NTU, developed the optical micromotion sensing system (M^2S^2) [45]. The M^2S^2 was embedded with a pair of orthogonally placed position-sensitive detectors (PSDs), as depicted in [45, Fig. 3]. The PSDs tracked the 3-D displacement of the tip of a microsurgical instrument in x-, y-, and z-axes, while the participants carried out some synthetic tasks that mimicked the maneuvers performed during a real microsurgical procedure. The tasks were carried out in the workspace of M^2S^2, which was a target platform of dimension $10\times10\times10$ mm^3, as depicted in [46, Figs. 1 and 2]. A stylus that had similar mass and design as a typical surgical forceps was designed with a small white reflector ball attached to its tip, as depicted in [46, Figs. 4 and 5]. When an IR diode illuminated the workspace, the 3-D position of the tip of the instrument was calculated using the centroid position of the reflected IR rays captured by the PSDs.

As the participants performed the tasks in the M^2S^2 workspace, for their visual feedback, a 19″ flat LCD TV screen was provided. The TV screen was placed 70 cm away from their seating position. The participants were asked to seat comfortably facing the TV screen and hold the stylus between their index and thumb fingers. They were also instructed to rest their wrist on the small platform of M^2S^2. The data were collected at 250 Hz with a data acquisition card (PD-MF-16-150, United Electronics Industries, USA) with a 16-bit resolution. For more details about the M^2S^2 design and data acquisition, the readers are referred to [44]–[46].

Overall, 54 tremor traces were recorded in 3-D, while the participants carried out the two tasks.

1) *Pointing:* The participants were asked to point at the center of the platform and maintain the position of the tip of the stylus at the set point for 30 s. For the visual feedback, two dots were displayed on the screen. One dot was stationary, and the other could be moved according to the position of the tip of the stylus. The subjects had to overlap the two dots to maintain the tooltip at the target position [44]. The pointing task was designed to approximate a typical step carried out in retinal surgery, where a surgeon braces the tool motionless against the sclera for a short duration before inserting it through a targeted area of the sclera to perform precise manipulations inside the eyeball [47].
2) *Tracing:* The participants were asked to trace a synthetic circle of 4-mm diameter with the speed, which was realistic to surgical manipulation as the subjects had surgical knowledge. At the beginning of the task, a white circle of 4-mm diameter was displayed on the screen, and the participants had to rotate the displayed dot on this fixed circle clockwise for 30 s [44]. This synthetic task was medically relevant and was designed to simulate the incision and vein tracing maneuvers [46], [47]. The vein tracing maneuver is often performed in a retinal surgery where a surgeon traces the curved retinal vein ($\approx$10 mm), choosing a speed comfortable to them [47].

B. Performance of the SSA Algorithm—Off-Line Analysis

We applied the off-line SSA algorithm on the data recorded in the xyz-axes independently. To select an optimal window size, we varied L from 15 to 200. Fig. 3 shows Accuracy (%) averaged across all subjects and the xyz-axes. It peaks at certain values of L. It has been suggested to separate the desired periodic or quasi-periodic signal from the mixture, $L \geq f_s/f_l$ [48]; where f_s is the sampling frequency and f_l is the lowest frequency present in the desired periodic or quasi-periodic signal. In our case, the lowest frequency component in the quasi-periodic tremor band is 6 Hz; hence, L should be ≥ 42. We obtained an average Accuracy (%) of 93.3% at $L = 42$ across all the subjects for both tasks. At $L = 20$ where the first peak occurred, the average Accuracy (%)

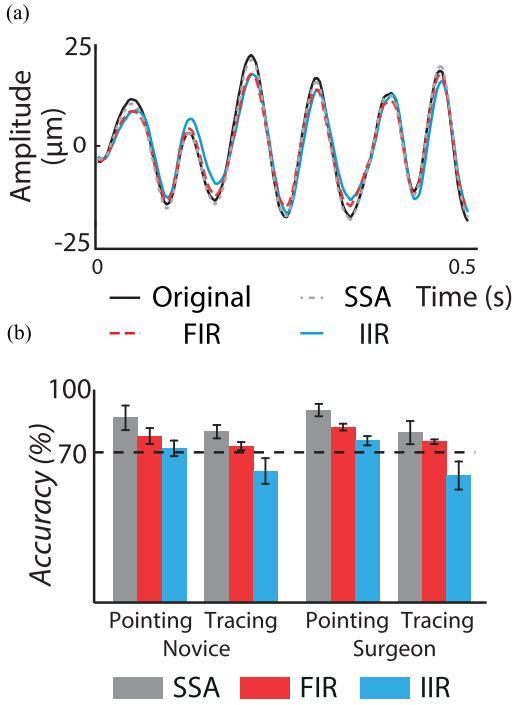

Fig. 4. (a) SSA filter provides closer approximation of the tremor signal compared with the conventional FIR and IIR filters. (b) Accuracy (%) averaged across each subject group. The SSA filter outperforms both FIR and IIR filters. The dashed line shows the minimum acceptable accuracy of 70%.

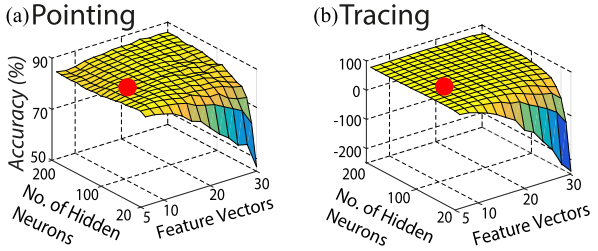

Fig. 5. Accuracy (%) averaged across all subjects for a range of variation of number of hidden neurons and feature vectors for (a) pointing task and (b) tracing task.

was 84.3%. The smallest L that can yield the desired accuracy is the optimal selection, as it leads to a reduced size of the covariance matrix in the SVD; hence, we chose $L = 20$.

The performance of the SSA algorithm was compared against conventional FIR and IIR low-pass filters. The SSA algorithm with $L = 20$ causes the fixed delay of 19 samples. To choose an FIR filter with a similar order, an FIR low-pass filter based on a Hamming window with a cutoff frequency of 5 Hz, and order 40 was chosen, which causes a time delay of 20 samples. The IIR Butterworth filter had a 5-Hz cutoff frequency and was of order 2. The lower order was chosen to minimize the phase delay, which is just 12 samples. The zero-phase filter with the same specifications as the IIR filter was used to extract the original tremor, which served as the ground truth.

Fig. 4(a) shows a 0.5-s plot of the approximated tremor data in the z-axis, obtained from three filters for the novice subject N1. It is evident that the SSA algorithm closely estimates the actual tremor compared with both conventional IIR and FIR filters. Fig. 4(b) shows a bar chart with averaged Accuracy (%) across each subject group. The SSA algorithm outperforms both FIR and IIR filters in both tasks. The IIR filter fails to achieve the required accuracy for the tracing task. This encouraged adoption of the RSSA-ELM setting for real-time filtering.

C. Selection of ELM Parameters

Before we proceed with the results of the RSSA-ELM method, we describe how the ELM algorithm was initialized. The performance of ELM depends on the optimum initialization of the parameters: 1) hidden neurons $\tilde{N}$; 2) feature vectors p; and 3) the number of off-line training samples N. We performed a grid search to determine the number of $\tilde{N}$ and p. Taking 80% of the total data for training and 20% for testing, the percentage accuracy was calculated for the eight-sample ahead prediction. The numbers $\tilde{N}$ and p were varied in the range $[20, 200]$ and $[6, 30]$, respectively. Fig. 5(a) and (b) shows Accuracy (%) averaged across all the subjects for both pointing and tracing tasks. The variation in Accuracy (%) between two extreme values of $\tilde{N}$ was around 1% for the pointing task and 2% for the tracing task. However, between two extreme values of p, the variation in Accuracy (%) was significant in both pointing task and tracing task. The optimal parameters of the ELM algorithm were identified as $\tilde{N} = 100$ and $p = 10$.

In real-time tremor cancellation, it is highly desirable to have the shortest possible processing delay to ensure faster correspondence and more intuitiveness. In this work, we aim to reduce the RSSA estimation delay by at least half, with the motivation to achieve the required performance within just a nine-sample (36 ms) delay. This delay is similar to the delay caused by the conventional IIR filters. Hence, the prediction horizon was set to 10. The optimal $\tilde{N}$ and p were utilized to compute the minimum size of N, and the output of RSSA was fed to the ELM algorithm sample-by-sample, as shown in Fig. 2. At each iteration, the latest $L - 1$ samples were separated for the testing, and the remaining initial samples were used for the training. The training was recursively performed with the arrival of each new sample, and the size of the training data was varied from 250 to 3000 samples. Fig. 6 shows Accuracy (%) averaged across both subject groups for the pointing and tracing tasks. The prediction performance improved significantly up to 750 samples in the pointing task and 2000 samples in the tracing task. In the tracing task, the prediction accuracy reaches to 70% only when $N \geq 2000$. Therefore, to achieve the required prediction performance in both tasks, for the majority of traces, the optimum N was set to 2000 (8 s).

D. Performance of the RSSA-ELM—Online Analysis

Fig. 7 illustrates a representative performance of the RSSA and RSSA-ELM algorithms on a short excerpt of data, recorded during the pointing task. As will be described later, for the RSSA algorithm, the estimation was performed at a nine-sample delay. Fig. 7(a) shows that the tremor fluctuations, riding on the voluntary motion, have been effectively attenuated with both the RSSA and RSSA-ELM algorithms.

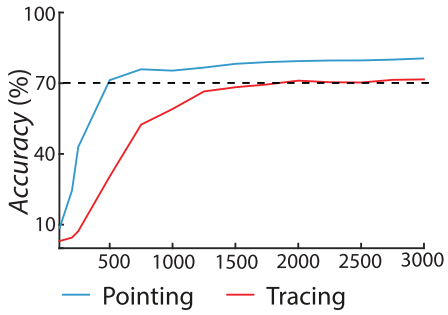

Fig. 6. Prediction Accuracy (%) of the ELM algorithm against the number of training samples, averaged across all subjects.

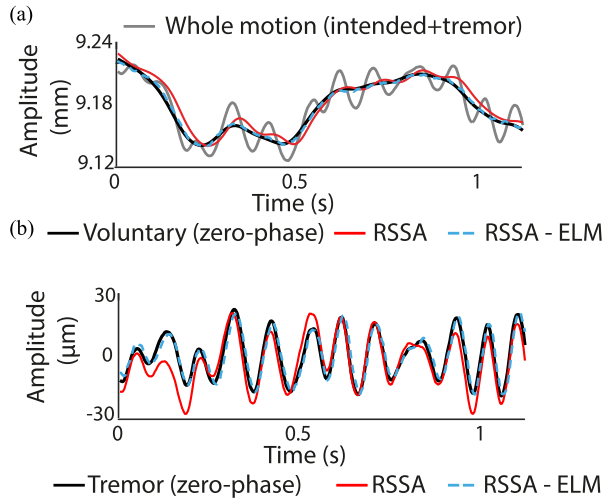

Fig. 7. Example for the performance of the RSSA and RSSA-ELM algorithms in approximating (a) intended and (b) tremor components of the whole motion signal.

We observe that the RSSA-ELM compensates better for the 36-ms delay than the RSSA method and closely tracks the intended motion, which was approximated by zero-phase filtering. Similarly, Fig. 7(b) shows that the RSSA-ELM algorithm tracks the actual tremor signal more successfully.

Fig. 8 shows the RMSE, obtained from both RSSA and RSSA-ELM at various delays. The RSSA-ELM outperforms the RSSA-only algorithm at all time delays, in all participants, in both pointing and tracing tasks. The RMSE of tremor estimation with the RSSA-ELM method is below the 10-μm threshold for most subjects even at very short time delays of 20 ms. Most conservatively, when the delay is 36 ms, the RSSA-ELM limits RMSE $\leq$ 10 μm, yielding $\geq$ 70% Accuracy (%), meeting both RMSE and Accuracy (%) requirements for all subjects. The overall performance was better in the pointing task that may reflect its simpler dynamics compared with the tracing task.

E. Moving Window RSSA-ELM

Fig. 9 shows the plots with Accuracy (%) obtained from the RSSA-ELM algorithm, averaged across the participants, and that achieved with the two proposed moving window algorithms, namely, the MW RSSA-ELM algorithm and the Enhanced MW RSSA-ELM algorithm. For delays as large as 36 ms, the performance of the RSSA-ELM algorithm matches that of the Enhanced MW RSSA-ELM algorithm. At 36-ms lag, the Enhanced MW RSSA-ELM algorithm provides 4% and 3% more accuracy than MW RSSA-ELM, for novice and surgeon pointing tasks. Similarly, it provides 10% better accuracy than the MW RSSA-ELM algorithm for tracing tasks of both subject groups. Beyond 36-ms lag, the savings achieved by the MW RSSA-ELM algorithm are at the expense of reduced accuracy. The Enhanced MW RSSA-ELM can recover this reduction only partially.

F. Computational Time

We quantified the computational time required by the RSSA-ELM, MW RSSA-ELM, and Enhanced MW RSSA-ELM algorithms as a function of the number of samples, as shown in Fig. 10. Our analysis was run on a PC with an Intel Core i5-4670 CPU (3.40 GHz) and 32-GB RAM and using MATLAB R2017a. In all algorithms, the delay was 36 ms, and the window size was kept to 8 s for both moving window algorithms. Crucially, the computational time taken by the RSSA-ELM method increases linearly with the data, whereas the time required by the moving window methods is almost fixed: 20 and 35 ms on average for Enhanced MW RSSA-ELM and MW RSSA-ELM, respectively.

G. Comparison With the Existing Methods

Finally, we compared the performance of the proposed Enhanced MW RSSA-ELM against the conventional FIR and IIR filters and the existing state-of-the-art MWLSSVM and 1D-OSRELM algorithms. A detailed description of the parameters optimization of MWLSSVM and 1D-OSRELM is provided separately in the Supplementary Material. For fairness in evaluation, the ELM predictor cascaded in the Enhanced MW RSSA-ELM to improve the performance was also appended with the conventional FIR and IIR filters and is referred to as FIR-ELM and IIR-ELM. In the FIR-ELM, IIR-ELM, and 1D-OSRELM algorithms, N was fixed to 2000 samples. Similarly, the moving window length of the Enhanced MW RSSA-ELM and MWLSSVM was also set to 2000 samples. In all five algorithms, with the arrival of every new sample, the output weights were updated, as detailed in Section III-B. For consistency in comparison, the performance of all the algorithms was evaluated at a nine-sample delay.

Fig. 11 depicts the averaged compensation Accuracy (%) obtained for all the subjects for the pointing and tracing tasks, which shows the superior performance of the proposed Enhanced MW RSSA-ELM algorithm compared with the existing methods. The proposed algorithm provided 80.21% Accuracy (%) in the pointing task compared with 73.83% and 72.03% Accuracy (%) obtained from the MWLSSVM and the 1D-OSRELM algorithm, respectively. Similarly, in the tracing task, the Enhanced MW RSSA-ELM algorithm yielded 10% better Accuracy (%) compared with the MWLSSVM algorithm, and it outperformed all the other algorithms. On average, over all the subjects and tasks, the Enhanced MW RSSA-ELM algorithm provided 74.54% Accuracy (%), which is 8.37% and 9.61% higher than the Accuracy (%)

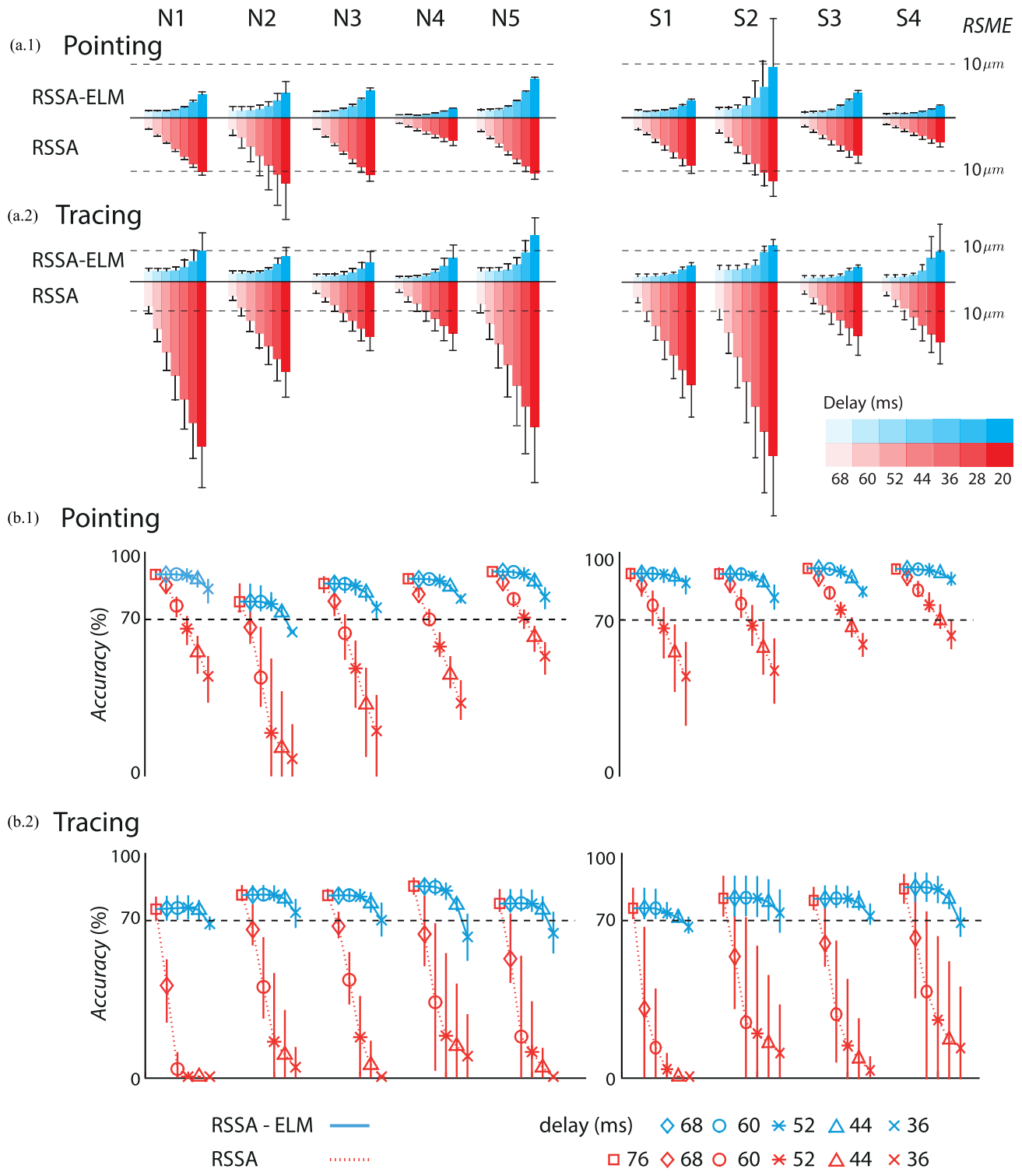

Fig. 8. Comparison between the RSSA and RSSA-ELM algorithms in terms of (a) RMSE and (b) Accuracy at various delay. The bars beyond the dashed line signify failure to keep the RMSE or Accuracy, below the 10 μm or above the 70% limits, respectively. The results suggest that the RSSA-ELM algorithm needs at least 36-ms delay to perform reliably in both tasks and in all subjects. Error bars represent the upper range: [mean, maximum]. (a.1) and (b.1) Pointing. (a.2) and (b.2) Tracing.

obtained with the MWLSSVM and 1D-OSRELM algorithms, respectively.

V. Discussion

The development of an efficient tremor cancellation method that can remove a surgeon's involuntary physiological tremor from the tip of a surgical instrument improves microsurgical performance radically. All the existing tremor compensating techniques use nonlinear phase prefiltering to isolate the tremor from the whole motion, which significantly distorts the filtered tremor signal and restricts the filtering accuracy. Although, in recent years, the phase correction methods have

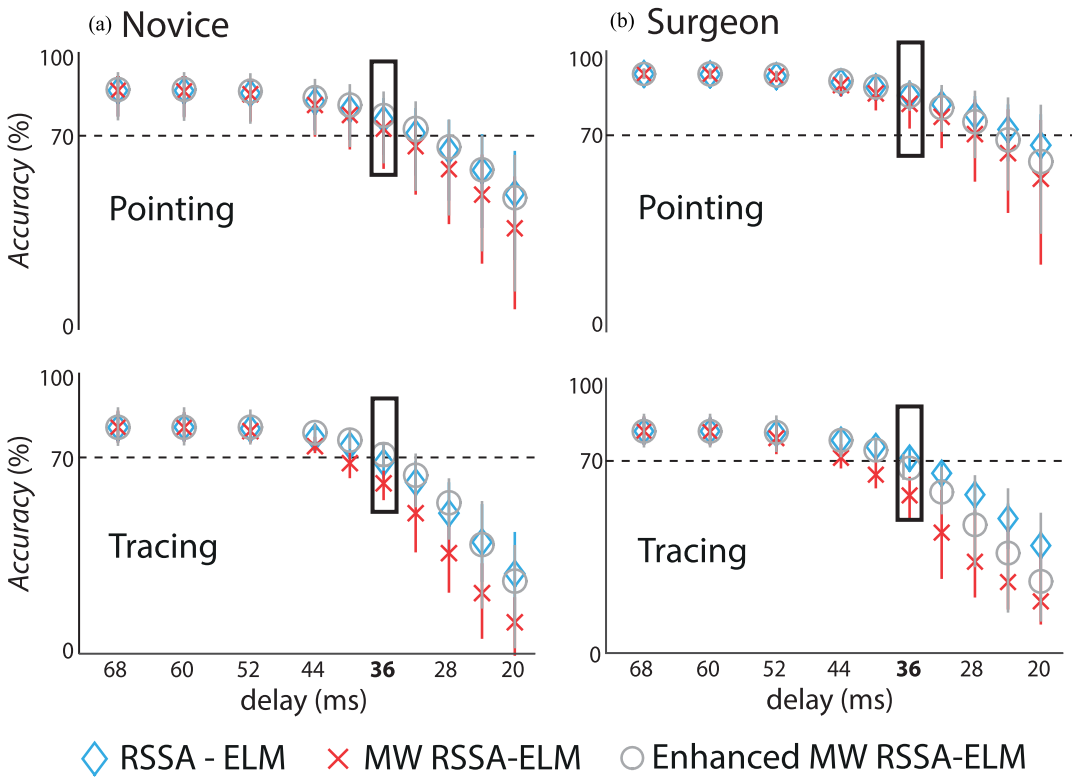

Fig. 9. Accuracy (%) obtained with RSSA-ELM, MW RSSA-ELM, and Enhanced MW RSSA-ELM, averaged across (a) novice subjects and (b) surgeons. Both moving window versions of the RSSA-ELM achieve the same performance as RSSA-ELM but at a significantly reduced computational cost. The black boxes show the performances at 36 ms. Error bars represent the range: [minimum, maximum].

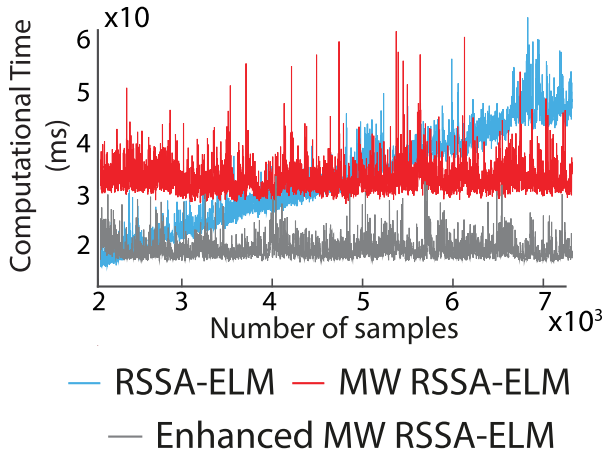

Fig. 10. Required computational time of the RSSA-ELM, MW RSSA-ELM, and Enhanced MW RSSA-ELM. The Enhanced MW RSSA-ELM achieves the same performance as the RSSA-ELM and MW RSSA-ELM but with a significantly lower computational time.

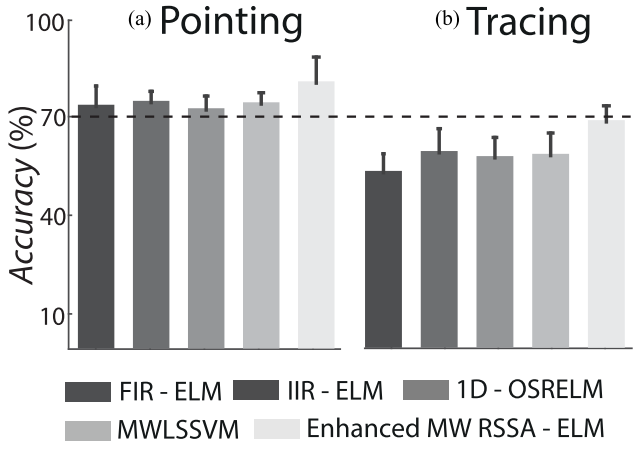

Fig. 11. Accuracy (%) obtained with the FIR-ELM, IIR-ELM, 1D-OSRELM, MWLSSVM, and Enhanced MW RSSA-ELM algorithms, averaged across (a) novice subjects and (b) surgeons. The Enhanced MW RSSA-ELM algorithm outperforms all the algorithms. Error bars represent the maximum range.

been proposed, those methods still utilized nonlinear phase filters to separate the tremor. Moreover, to rectify the distorted phase, those methods needed zero-phase filtering, which significantly limits their feasibility for real-time implementation. In our preliminary work, we had studied the viability of the standard RSSA-only algorithm to filter the tremor signal without causing any phase distortion. In this work, we have applied algorithmic improvement to the standard RSSA algorithm to reduce the computational cost while keeping the performance the same. We exploited the zero-phase characteristics of this modified RSSA algorithm to develop a combined estimator-predictor-based RSSA-ELM framework to directly extract the voluntary motion and the tremor from the whole motion, without the need of any prefiltering or zero-phase filtering. This is the main distinctiveness of the proposed framework.

We have uniquely formulated the RSSA-ELM structure such that, at every iteration, the last $L-1$ corrupted samples coming

from the RSSA estimator were discarded, and only the rest of the nondistorted samples were fed to the ELM predictor. Thus, the RSSA estimator offered zero-phase type filtering but with the transient delay of 19 samples (76 ms). The ELM predictor then learned the accurate signal fed from the RSSA estimator and made a forward prediction to shorten this delay to nine samples (36 ms) only. Since the hand tremor is a nonstationary signal and its characteristics vary continuously, this continual feed of the actual tremor signal to the ELM predictor enabled it to constantly track and predict the tremor signal accurately. Therefore, the proposed framework is dynamic, in contrast to the phase correction techniques that could track the tremor signal offline only. This is a major advantage of the proposed RSSA-ELM framework.

The cascaded RSSA-ELM framework suppressed the undesired tremulous motion below 10 μm, yielding an estimation accuracy of over 70%. In a pseudo-real-time implementation, it can achieve this performance at only a nine-sample (36 ms) delay. In addition, we proposed two moving window variants of the RSSA-ELM algorithm. These moving window algorithms iteratively operate on a fixed number of samples so that the computation time is constant regardless of the input data length. We showed that, on average, the Enhanced MW RSSA-ELM algorithm provided 3.5% and 10% better performance than the MW RSSA-ELM algorithm in the pointing and tracing tasks. The computational cost of the Enhanced MW RSSA-ELM algorithm is 1.5 times less compared with the MW RSSA-ELM algorithm. The Enhanced MW RSSA-ELM algorithm outperformed the conventional FIR and IIR filters and the state-of-the-art MWLSSVM and 1D-OSRELM algorithms. As such, the proposed framework exceeds the industry standard considerably.

Nonetheless, the proposed framework showed superior performance in a real-time emulation, and the extensive experimental testing and verification are crucial for a complete implementation of the proposed framework in a real surgical instrument. In addition, the extent of compensation entirely depends on the manipulator that controls the actuation of the tooltip. Full compensation cannot be achieved if the erroneous motion is larger than the manipulator range of motion.

Due to the efficient learning rate, the ELM algorithm is gaining popularity in the hardware implementations that require frequent on-chip training [49]–[51]. Therefore, the proposed Enhanced MW RSSA-ELM algorithm is suitable to implement in surgical hand-held tools, such as Micron and its descendant ITrem, for cancellation of tremor in real-time. The RSSA estimator and ELM predictor algorithms were used in this proof-of-concept study to show the potential of the proposed estimation–prediction framework. The proposed framework can be readily adapted to any other suitable estimator that offers zero-phase filtering similar to RSSA and any other machine learning predictor that provides simple yet efficient learning as ELM.

VI. Conclusion

We have revisited a long-standing problem in the existing research and offered a novel estimator-predictor-based RSSA-ELM framework that does not require prefiltering, unlike the existing methods. The proposed algorithm can attenuate the undesired tremor below 10 μm and yield filtering accuracy over 70% at only a nine-sample (36 ms) delay. For real-time implementation, we proposed two variants of the moving window RSSA-ELM algorithm. The Enhanced MW RSSA-ELM algorithm provides 6.75% more Accuracy (%) and is 1.5 times faster than the MW RSSA-ELM algorithm. The Enhanced MW RSSA-ELM also outperforms the conventional FIR and IIR filters and beats the performance of the existing state-of-the-art MWLSSVM algorithm by 8.37%.

Our future work includes quaternion extension of the proposed 1-D RSSA-ELM framework for real-time tremor filtering since the quaternion adaptive filters have shown improved performance compared with their 1-D versions [52]–[54]. We have previously presented the quaternion modeling and prediction algorithm for off-line tremor filtering in [31], [55], and [56].

Acknowledgment

The authors would like to thank Dr. Wei Tech Ang at Nanyang Technological University, Singapore, for the provision of the data. They would also like to thank two unknown reviewers for their insightful comments and suggestions that led to significantly improve the quality of this article.

The Matlab implementation codes of the recursive singular spectrum analysis (RSSA)-extreme learning machine (ELM) algorithms supporting this publication is openly available at https://doi.org/10.25405/data.ncl.13280501. Please contact Newcastle Research Data Service at rdm@ncl.ac.uk for access instructions.

References

[1] G. Deuschl, J. Raethjen, M. Lindemann, and P. Krack, "The pathophysiology of tremor," *Muscle Nerve*, vol. 24, no. 6, pp. 716–735, 2001.

[2] C. N. Riviere, R. S. Rader, and N. V. Thakor, "Adaptive cancelling of physiological tremor for improved precision in microsurgery," *IEEE Trans. Biomed. Eng.*, vol. 45, no. 7, pp. 839–846, Jul. 1998.

[3] C. N. Riviere, J. Gangloff, and M. de Mathelin, "Robotic compensation of biological motion to enhance surgical accuracy," *Proc. IEEE*, vol. 94, no. 9, pp. 1705–1716, Sep. 2006.

[4] Y. S. Kwoh, J. Hou, E. A. Jonckheere, and S. Hayati, "A robot with improved absolute positioning accuracy for CT guided stereotactic brain surgery," *IEEE Trans. Biomed. Eng.*, vol. BE-35, no. 2, pp. 153–160, Feb. 1988.

[5] I. W. Hunter *et al.*, "A teleoperated microsurgical robot and associated virtual environment for eye surgery," *Presence, Teleoperators Virtual Environ.*, vol. 2, no. 4, pp. 265–280, Jan. 1993.

[6] C. N. Riviere and N. V. Thakor, "Modeling and canceling tremor in human-machine interfaces," *IEEE Eng. Med. Biol. Mag.*, vol. 15, no. 3, pp. 29–36, May/Jun. 1996.

[7] W. Tech Ang, P. K. Khosla, and C. N. Riviere, "Design of all-accelerometer inertial measurement unit for tremor sensing in hand-held microsurgical instrument," in *Proc. IEEE Int. Conf. Robot. Autom.*, vol. 2, Sep. 2003, pp. 1781–1786.

[8] M. Patkin, "Ergonomics applied to the practice of microsurgery," *Austral. New Zealand J. Surg.*, vol. 47, pp. 320–329, Jun. 1977.

[9] R. C. Harwell and R. L. Ferguson, "Physiologic tremor and microsurgery," *Microsurgery*, vol. 4, no. 3, pp. 187–192, 1983.

[10] S. Charles, "Dexterity enhancement for surgery," in *Computer Integrated Surgery: Technology and Clinical Applications*, R. H. Taylor, S. Lavallée, G. C. Burdea, and E. R. Mösges, Eds. Cambridge, MA, USA: MIT Press, 1996, pp. 467–471.

[11] W. M. Tang and D. P. Han, "A study of surgical approaches to retinal vascular occlusions," *Arch. Ophthalmol.*, vol. 118, pp. 138–143, Jan. 2000.
[12] T. S. Wells, R. A. MacLachlan, and C. N. Riviere, "Toward hybrid position/force control for an active handheld micromanipulator," in *Proc. IEEE Int. Conf. Robot. Autom. (ICRA)*, May 2014, pp. 772–777.
[13] Y. N. Aye, S. Zhao, and W. T. Ang, "An enhanced intelligent handheld instrument with visual servo control for 2-DOF hand motion error compensation," *Int. J. Adv. Robotic Syst.*, vol. 10, no. 10, p. 355, Jan. 2013.
[14] R. H. Taylor *et al.*, "A telerobotic assistant for laparoscopic surgery," *IEEE Eng. Med. Biol. Mag.*, vol. 14, no. 3, pp. 279–288, May/Jun. 1995.
[15] G. H. Ballantyne and F. Moll, "The da Vinci telerobotic surgical system: The virtual operative field and telepresence surgery," *Surg. Clin. North Amer.*, vol. 83, no. 6, pp. 1293–1304, 2003.
[16] G. Dogangil, B. L. Davies, and F. R. Y. Baena, "A review of medical robotics for minimally invasive soft tissue surgery," *Proc. Inst. Mech. Eng. H, J. Eng. Med.*, vol. 224, no. 5, pp. 653–679, May 2009.
[17] R. Taylor *et al.*, "A steady-hand robotic system for microsurgical augmentation," *Int. J. Robot. Res.*, vol. 18, no. 12, pp. 1201–1210, Dec. 1999.
[18] B. Gonenc, J. Handa, P. Gehlbach, R. H. Taylor, and I. Iordachita, "A comparative study for robot assisted vitreoretinal surgery: Micron vs. the steady-hand robot," in *Proc. IEEE Int. Conf. Robot. Autom.*, May 2013, pp. 4832–4837.
[19] C. N. Riviere, W. Tech Ang, and P. K. Khosla, "Toward active tremor canceling in handheld microsurgical instruments," *IEEE Trans. Robot. Autom.*, vol. 19, no. 5, pp. 793–800, Oct. 2003.
[20] W. T. Latt, U.-X. Tan, C. Y. Shee, C. N. Riviere, and W. T. Ang, "Compact sensing design of a handheld active tremor compensation instrument," *IEEE Sensors J.*, vol. 9, no. 12, pp. 1864–1871, Dec. 2009.
[21] C. Bergeles and G.-Z. Yang, "From passive tool holders to microsurgeons: Safer, smaller, smarter surgical robots," *IEEE Trans. Biomed. Eng.*, vol. 61, no. 5, pp. 1565–1576, May 2014.
[22] K. J. W. Craik, "Theory of the human operator in control systems: I. Tsshe operator as an engineering system," *Brit. J. Psychol. Gen. Sect.*, vol. 38, no. 2, pp. 56–61, Dec. 1947.
[23] P. O. Riley and M. J. Rosen, "Evaluating manual control devices for those with tremor disability," *J. Rehabil. Res. Develop.*, vol. 24, no. 2, pp. 99–110, Jan. 1987.
[24] M. Javidan, J. Elek, and A. Prochazka, "Attenuation of pathological tremors by functional electrical stimulation II: Clinical evaluation," *Ann. Biomed. Eng.*, vol. 20, no. 2, pp. 225–236, Mar. 1992.
[25] A. V. Oppenheim and R. W. Schaefer, *Discrete-Time Signal Processing*. Bergen Country, NJ, USA: Prentice-Hall, 2001.
[26] C. N. Riviere, R. S. Rader, and P. K. Khosla, "Characteristics of hand motion of eye surgeons," in *Proc. 19th Annu. Int. Conf. IEEE Eng. Med. Biol. Soc.*, Nov. 1997, pp. 1690–1693.
[27] S. Tatinati, K. C. Veluvolu, S.-M. Hong, W. T. Latt, and W. T. Ang, "Physiological tremor estimation with autoregressive (AR) model and Kalman filter for robotics applications," *IEEE Sensors J.*, vol. 13, no. 12, pp. 4977–4985, Dec. 2013.
[28] K. C. Veluvolu, W. T. Latt, and W. T. Ang, "Double adaptive bandlimited multiple Fourier linear combiner for real-time estimation/filtering of physiological tremor," *Biomed. Signal Process. Control*, vol. 5, no. 1, pp. 37–44, Jan. 2010.
[29] K. C. Veluvolu and W. T. Ang, "Estimation of physiological tremor from accelerometers for real-time applications," *Sensors*, vol. 11, no. 3, pp. 3020–3036, Mar. 2011.
[30] K. C. Veluvolu, S. Tatinati, S.-M. Hong, and W. T. Ang, "Multistep prediction of physiological tremor for surgical robotics applications," *IEEE Trans. Biomed. Eng.*, vol. 60, no. 11, pp. 3074–3082, Nov. 2013.
[31] K. Adhikari, S. Tatinati, W. T. Ang, K. C. Veluvolu, and K. Nazarpour, "A quaternion weighted Fourier linear combiner for modeling physiological tremor," *IEEE Trans. Biomed. Eng.*, vol. 63, no. 11, pp. 2336–2346, Nov. 2016.
[32] S. Tatinati, K. C. Veluvolu, and W. Tech Ang, "Multistep prediction of physiological tremor based on machine learning for robotics assisted microsurgery," *IEEE Trans. Cybern.*, vol. 45, no. 2, pp. 328–339, Feb. 2015.
[33] S. Tatinati, K. Nazarpour, W. T. Ang, and K. C. Veluvolu, "Multidimensional modeling of physiological tremor for active compensation in handheld surgical robotics," *IEEE Trans. Ind. Electron.*, vol. 64, no. 2, pp. 1645–1655, Feb. 2017.
[34] N. Golyandina and A. Zhigljavsky, *Singular Spectrum Analysis for Time Series*. Berlin, Germany: Springer-Verlag, 2013.
[35] G.-B. Huang, H. Zhou, X. Ding, and R. Zhang, "Extreme learning machine for regression and multiclass classification," *IEEE Trans. Syst., Man, Cybern. B, Cybern.*, vol. 42, no. 2, pp. 513–529, Apr. 2012.
[36] K. Adhikari, S. Tatinati, K. C. Veluvolu, J. A. Chambers, and K. Nazarpour, "Real-time physiological tremor estimation using recursive singular spectrum analysis," in *Proc. 39th Annu. Int. Conf. IEEE Eng. Med. Biol. Soc.*, Jul. 2017, pp. 3202–3205.
[37] G.-B. Huang, Q.-Y. Zhu, and C.-K. Siew, "Extreme learning machine: A new learning scheme of feedforward neural networks," in *Proc. IEEE Int. Joint Conf. Neural Netw.*, Jul. 2004, pp. 985–990.
[38] H.-X. Tian and Z.-Z. Mao, "An ensemble ELM based on modified AdaBoost.RT algorithm for predicting the temperature of molten steel in ladle furnace," *IEEE Trans. Autom. Sci. Eng.*, vol. 7, no. 1, pp. 73–80, Jan. 2010.
[39] Y. Yu, T.-M. Choi, and C.-L. Hui, "An intelligent quick prediction algorithm with applications in industrial control and loading problems," *IEEE Trans. Autom. Sci. Eng.*, vol. 9, no. 2, pp. 276–287, Apr. 2012.
[40] S. B. Sulistyo, D. Wu, W. L. Woo, S. S. Dlay, and B. Gao, "Computational deep intelligence vision sensing for nutrient content estimation in agricultural automation," *IEEE Trans. Autom. Sci. Eng.*, vol. 15, no. 3, pp. 1243–1257, Jul. 2018.
[41] E. Skordilis and R. Moghaddass, "A double hybrid state-space model for real-time sensor-driven monitoring of deteriorating systems," *IEEE Trans. Autom. Sci. Eng.*, vol. 17, no. 1, pp. 72–87, Jan. 2020.
[42] O. Haavisto, "Detection and analysis of oscillations in a mineral flotation circuit," *Control Eng. Pract.*, vol. 18, no. 1, pp. 23–30, Jan. 2010.
[43] S. Enshaeifar, S. Kouchaki, C. C. Took, and S. Sanei, "Quaternion singular spectrum analysis of electroencephalogram with application in sleep analysis," *IEEE Trans. Neural Syst. Rehabil. Eng.*, vol. 24, no. 1, pp. 57–67, Jan. 2016.
[44] E. L. M. Su, T. L. Win, W. T. Ang, T. C. Lim, C. L. Teo, and E. Burdet, "Micromanipulation accuracy in pointing and tracing investigated with a contact-free measurement system," in *Proc. Annu. Int. Conf. IEEE Eng. Med. Biol. Soc.*, Sep. 2009, pp. 3960–3963.
[45] T. L. Win, U. X. Tan, C. Y. Shee, and W. T. Ang, "Design and calibration of an optical micro motion sensing system for micromanipulation tasks," in *Proc. IEEE Int. Conf. Robot. Autom.*, Apr. 2007, pp. 3383–3388.
[46] W. T. Latt, U. X. Tan, K. C. Veluvolu, J. K. D. Lin, C. Y. Shee, and W. T. Angs, "System to assess accuracy of micromanipulation," in *Proc. 29th Annu. Int. Conf. IEEE Eng. Med. Biol. Soc.*, Aug. 2007, pp. 5743–5746.
[47] B. C. Becker, "Vision-based control handheld micromanipulator for robot-assited retinal surgery," Ph.D. dissertation, School Comput. Sci., Robot. Inst., Carnegie Mellon Univ., Pittsburgh, PA, USA, 2012.
[48] F. Ghaderi, H. R. Mohseni, and S. Sanei, "Localizing heart sounds in respiratory signals using singular spectrum analysis," *IEEE Trans. Biomed. Eng.*, vol. 58, no. 12, pp. 3360–3367, Dec. 2011.
[49] M. Bataller-Mompean *et al.*, "Support tool for the combined Software/Hardware design of on-chip ELM training for SLFF neural networks," *IEEE Trans. Ind. Informat.*, vol. 12, no. 3, pp. 1114–1123, Jun. 2016.
[50] E. Yao and A. Basu, "VLSI extreme learning machine: A design space exploration," *IEEE Trans. Very Large Scale Integr. (VLSI) Syst.*, vol. 25, no. 1, pp. 60–74, Jan. 2017.
[51] M. Rasouli, Y. Chen, A. Basu, S. L. Kukreja, and N. V. Thakor, "An extreme learning machine-based neuromorphic tactile sensing system for texture recognition," *IEEE Trans. Biomed. Circuits Syst.*, vol. 12, no. 2, pp. 313–325, Apr. 2018.
[52] C. C. Took and D. P. Mandic, "The quaternion LMS algorithm for adaptive filtering of hypercomplex processes," *IEEE Trans. Signal Process.*, vol. 57, no. 4, pp. 1316–1327, Apr. 2009.
[53] C. Cheong Took and D. P. Mandic, "A quaternion widely linear adaptive filter," *IEEE Trans. Signal Process.*, vol. 58, no. 8, pp. 4427–4431, Aug. 2010.
[54] C. Jahanchahi and D. P. Mandic, "A class of quaternion Kalman filters," *IEEE Trans. Neural Netw. Learn. Syst.*, vol. 25, no. 3, pp. 533–544, Mar. 2014.
[55] K. Adhikari, S. Tatinati, K. C. Veluvolu, and K. Nazarpour, "Modeling 3D tremor signals with a quaternion weighted Fourier linear combiner," in *Proc. 7th Int. IEEE/EMBS Conf. Neural Eng. (NER)*, Apr. 2015, pp. 799–802.
[56] Y. Wang *et al.*, "Multi-step prediction of physiological tremor with random quaternion neurons for surgical robotics applications," *IEEE Access*, vol. 6, pp. 42216–42226, 2018.

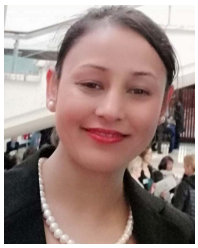

Kabita Adhikari received the B.Eng. degree in electronics and communication engineering from the Institute of Engineering, Pulchowk Campus, Tribhuvan University, Dharan, Nepal, in 2004, the M.Sc. degree from Northumbria University, Newcastle upon Tyne, U.K., in 2007, and the Ph.D. degree from Newcastle University, Newcastle upon Tyne, in 2019.

From 2008 to 2010, she was a Lecturer with the South Tyneside College, South Shields, U.K. She then joined Newcastle University in 2010 as a Teaching Fellow. Since 2019, she has been a Lecturer with the School of Engineering, Newcastle University. Her research interests lie primarily in the areas of intelligent signal processing, machine learning, preventive and predictive modeling for biomedical applications, AI-enabled assistive health-care technologies, and robotics.

Sivanagaraja Tatinati (Member, IEEE) received the B.Tech. degree in electronics and communication engineering from Acharya Nagarjuna University, Guntur, India, in 2010, and the Ph.D. degree from the School of Electronics Engineering, Kyungpook National University, Daegu, South Korea, in 2016.

He held a post-doctoral position at the School of Computer Science, Kyugnpook National University, in 2016. Since 2017, he has been a Research Fellow with the School of Electrical and Electronics Engineering, Nanyang Technological University, Singapore. His current research areas include machine learning, data analytics, natural language processing and generation, and robotics technology for biomedical applications.

Kalyana C. Veluvolu (Senior Member, IEEE) received the B.Tech. degree in electrical and electronic engineering from Acharya Nagarjuna University, Guntur, India, in 2002, and the Ph.D. degree in electrical engineering from Nanyang Technological University, Singapore, in 2006.

From 2006 to 2009, he was a Research Fellow with the Bio-Robotics Group, Robotics Research Center, Nanyang Technological University. Since 2009, he has been with the School of Electronics Engineering, Kyungpook National University, Daegu, South Korea, where he is currently a Professor. He was a Visiting Professor with the School of Mechanical and Aerospace Engineering, Nanyang Technological University, from 2016 to 2017. He has also held several visiting positions in the Newcastle University, Newcastle upon Tyne, U.K., and the University of Valenciennes, Valenciennes, France. He has been a principal investigator or a co-investigator on a number of research projects funded by government, industry, and universities. He has authored or coauthored over 130 journal and conference proceedings articles. His current research interests include nonlinear estimation and filtering, sliding mode control, brain–computer interface, autonomous vehicles, biomedical signal processing, and surgical robotics.

Dr. Veluvolu received several awards for research excellence, including the 2020 KNU Academic Award and the Excellent Research Award from the Ministry of Education, South Korea, in 2018. He is also an Associate Editor of the *Journal of The Franklin Institute*, *Systems Science and Control Engineering*, and *Electronics*. He has been on technical/program committees of several international conferences.

Jonathon A. Chambers (Fellow, IEEE) received the Ph.D. and D.Sc. degrees in signal processing from the Imperial College of Science, Technology and Medicine (Imperial College London), London, U.K., in 1990 and 2014, respectively.

From 1991 to 1994, he was a Research Scientist with the Schlumberger Cambridge Research Center, Cambridge, U.K. In 1994, he returned to Imperial College London as a Lecturer in signal processing and was promoted to Reader (Associate Professor) in 1998. From 2001 to 2004, he was the Director of the Center for Digital Signal Processing and a Professor of signal processing with the Division of Engineering, King's College London, London. From 2004 to 2007, he was a Cardiff Professorial Research Fellow with the School of Engineering, Cardiff University, Cardiff, U.K. From 2007 to 2014, he led the Advanced Signal Processing Group, School of Electronic, Electrical and Systems Engineering, Loughborough University, Loughborough, where he is currently a Visiting Professor. In 2015, he joined the School of Electrical and Electronic Engineering, Newcastle University, Newcastle upon Tyne, U.K., where he was a Professor of signal and information processing and led the ComS2IP Group and is also a Visiting Professor. In 2017, he became the Head of the School of Engineering, University of Leicester, Leicester, U.K. He is also an International Honorary Dean and a Guest Professor with Harbin Engineering University, Harbin, China, with support from the 1000 Talents Scheme. He is a coauthor of the books: *Recurrent Neural Networks for Prediction: Learning Algorithms, Architectures and Stability* (New York, NY, USA: Wiley, 2001) and *EEG Signal Processing* (New York: Wiley, 2007). He has advised more than 90 researchers through to Ph.D. graduation and has authored/coauthored more than 500 conference papers and journal articles; many of them are in the IEEE journals. His research interests include adaptive signal processing, and machine learning, and their applications.

Dr. Chambers is a fellow of the Royal Academy of Engineering, U.K., and the Institution of Electrical Engineers. In 2007, he received the first QinetiQ Visiting Fellowship for his outstanding contributions to adaptive signal processing and his contributions to QinetiQ, as a result of his successful industrial collaboration with the international defense systems company QinetiQ. He was the Technical Program Chair of the 15th International Conference on Digital Signal Processing and the 2009 IEEE Workshop on Statistical Signal Processing, both held at Cardiff, U.K., and the Technical Program Co-Chair of the 36th IEEE International Conference on Acoustics, Speech, and Signal Processing, Prague, Czech Republic. He has served on the IEEE Signal Processing Theory and Methods Technical Committee for six years and the IEEE Signal Processing Society Awards Board for three years, together with the Jack Kilby Award Committee. He was an Associate Editor for the IEEE TRANSACTIONS ON SIGNAL PROCESSING for two terms over the periods 1997–1999 and 2004–2007 and as a Senior Area Editor from 2011 to 2014.